Volume 86 • Issue 1 • January 2018

Journal of Achievements in Materials and Manufacturing Engineering

International Scientific Journal published monthly by the World Academy of Materials and Manufacturing Engineering

Nano-structured (Mo,Ti)C-C-Ni magnetic powder

S.M. Kaczmarek [a], A. Biedunkiewicz [b], T. Bodziony [a], P. Figiel [b,*], T. Skibiński [a], M. Krawczyk [c], U. Gabriel-Półrolniczak [d]

[a] Institute of Physics, Faculty of Mechanical Engineering and Mechatronics, West Pomeranian University of Technology, Szczecin, Al. Piastów 48, 70-311 Szczecin, Poland

[b] Institute of Materials Science and Engineering, Faculty of Mechanical Engineering and Mechatronics, West Pomeranian University of Technology, Szczecin, Al. Piastów 19, 70-310 Szczecin, Poland

[c] Institute of Manufacturing Engineering, Faculty of Mechanical Engineering and Mechatronics, West Pomeranian University of Technology, Szczecin, Al. Piastow 19, 70-310 Szczecin, Poland

[d] Institute of Transport Engineering, Faculty of Transport Engineering and Economics, Maritime University of Szczecin, Al. Pobożnego 11, 70-507 Szczecin, Poland

* Corresponding e-mail address: pfigiel@zut.edu.pl

ABSTRACT

Purpose: The paper presents the results of phase composition and magnetic properties of Mo-Ni-Ti-C nanostructured powders. The aim of this research is understanding the correlation between key magnetic properties and the parameters that influence them in the nanostructured powders from Mo-Ni-Ti-C system.

Design/methodology/approach: The powder samples were synthesised using modified sol-gel method. Obtained powder were subjected for composition and magnetic properties in a wide temperature range by means of Electron Paramagnetic Resonance (EPR) and magnetic susceptibility measurements. To study the phase composition X-ray diffraction were performed. The morphology of the powders were investigated by scanning electron microscopy (SEM).

Findings: Different kinds of structural and magnetic phases have been found in the investigated compounds, e.g. (Mo, Ti)C, C, Ni. It was found that such different phases create different kinds of magnetic interactions, from paramagnetic, antiferromagnetic up to superparamagnetic. Significant magnetic anisotropy has been revealed for low temperatures, which lowers with temperature increase. Moreover, non-usual increasing of the magnetization as a function of temperature was observed. It suggests, that overall long-range AFM interaction may be responsible for the magnetic properties.

Research limitations/implications: For the future work explanation which phases in Mo-Ni-Ti-C system are responsible for different kinds of magnetic interactions are planned.

Practical implications: The composition of different kinds of phases may be controlled to tune magnetic properties of the nanostructured Mo-Ni-Ti-C systems.

Originality/value: In this study, for the first time Mo-Ni-Ti-C nanostructured samples were prepared with different kinds of structural and magnetic phases, creating different kinds of magnetic interactions, from paramagnetic, antiferromagnetic up to superparamagnetic-like. The latter seems to be formed due to the presence of magnetic nanoparticles and long-range antiferromagnetic interactions dominating in the whole temperature range.

Keywords: Nanopowder, Mo-Ni-Ti-C systems, Magnetic susceptibility, EPR measurements, Magnetic anisotropy, Antiferromagnetism, Superparamagnetism

Reference to this paper should be given in the following way:

S.M. Kaczmarek, A. Biedunkiewicz, T. Bodziony, P. Figiel, T. Skibiński, M. Krawczyk, U. Gabriel-Półrolniczak, Nano-structured (Mo,Ti)C-C-Ni magnetic powder, Journal of Achievements in Materials and Manufacturing Engineering 86/1 (2018) 5-13.

MATERIALS

1. Introduction

Nanostructural materials have often unique chemical, structural, electrical, and magnetic properties [1-8], with potential applications including: information storage, color imaging, bioprocessing, magnetic refrigeration and ferrofluids [9-15]. The materials exhibit unique type of disorder, with very-low-energy regions (crystallites) existing at the expense of higher-energy boundary, interface, or surface regions. Magnetic nanoparticles and nanostructured studies combine a broad range of synthetic and investigative techniques from physics, chemistry, and materials science.

Molybdenum carbides, like Mo_2C, MoC_{1-x}, bi-carbide type (Mo,Ti)C, TiC/MoC and MoC/Mo_2C „core-shell" type composites [16-21], due to their important, recently uncovered magnetic properties, pose unknown yet knowledge capability about magnetism in materials. Recently, permanently growing interest is attached to (Mo,Ti)C composites (stable solution on the basis of Ni) due to their specific chemo-mechanical properties [18,20,22-32].

The object of our research in the paper are nanostructured powders belonging to a Mo-Ni-Ti-C system, that comprise richness of crystallic and magnetic phases being a source of different magnetic interactions like paramagnetism, ferromagnetism, antiferromagnetism and superparamagnetism. The interactions appear at different temperature ranges while their supremacy depends on a kind of substrates used in the synthesis. The aim of the paper is understanding the correlation between key magnetic properties and the parameters that influence them in the nanostructured powders from Mo-Ni-Ti-C system.

2. Materials and methodology

The following Mo-Ni-Ti-C samples were prepared and investigated for their phase composition and magnetic properties [33] (Tab. 1).

Table 1.
Samples, their composition and investigations

Sample No.	Chemical composition	Phase content after synthesis	Average size of (Ti,Mo)C crystallites, nm
1	Mo, Ti, C	(Mo,Ti)C + graphite (C)	40
2	Mo, Ti, Ni, C	(Mo,Ti)C + graphite (C) + 3wt.% Ni	100
3	Mo, Ti, Ni, C	(Mo,Ti)C + graphite (C) + 40wt.% Ni	100

Phase content was analyzed using XRD method based on PW3040/60 X´Pert Pro of PANalytical B.V. An average crystallite sizes were calculated by the Scherrer`s formula [31]. The morphology of nanopowders was analyzed by Scanning Electron Microscopy (SEM) apparatus of HITACHI SU.

Magnetic resonance experiment was performed by using conventional X–band Bruker ELEXSYS E 500 CW–spectrometer operating at 9.5 GHz with 100 kHz magnetic field modulation. The first derivative of the absorption spectra has been recorded as a function of the applied magnetic field within a 0-1.4 T range. Temperature dependences of the spectra were recorded by using Oxford Instrument ESP helium-, nitrogen-flow cryostat in a range of 3-300 K.

The static (dc) magnetic susceptibility measurements were carried out using a Quantum Design MPMS XL–7 magnetometer (SQUID) with EverCool Magnetic Property Measurement System. The temperature range was 4-300 K and magnetic fields up to 70 kOe in field cooling (FC) and zero field cooling (ZFC) regimes.

3. Results

3.1. XRD measurements

As one can see from Figure 1 the nanostructured powders are multiphase. The analysis of phase composition performed by XRD method indicated presence the carbide of (Mo,Ti)C type, graphite, while in case of samples No. 2 and 3 also nickel (Ni). The peak intensity of nickel increased significantly with increasing amount of nickel in the powder

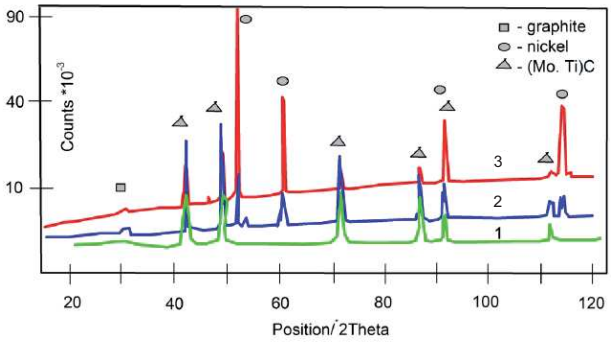

Fig. 1. The XRD patterns of nanostructured powders: sample 1, 2 and 3

3.2. SEM investigations

Figures 2, 3 and 4 show SEM images of the nano-structured samples. As can be seen the powders are inhomogeneous and multiphase as was concluded above from XRD measurements.

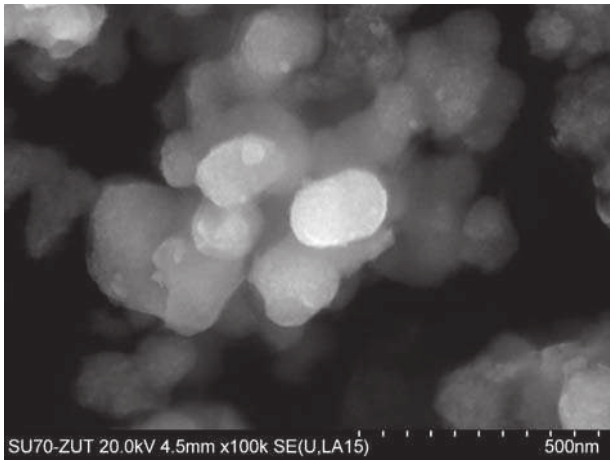

Fig. 2. Morphology of the sample No. 1. (Mo-Ti-C sytem)

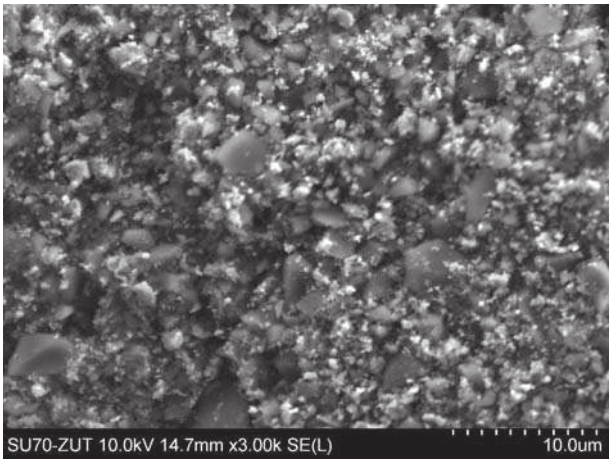

Fig. 3. Morphology of the sample No. 2. Mo-Ni-Ti-C system (3 wt.% of Ni)

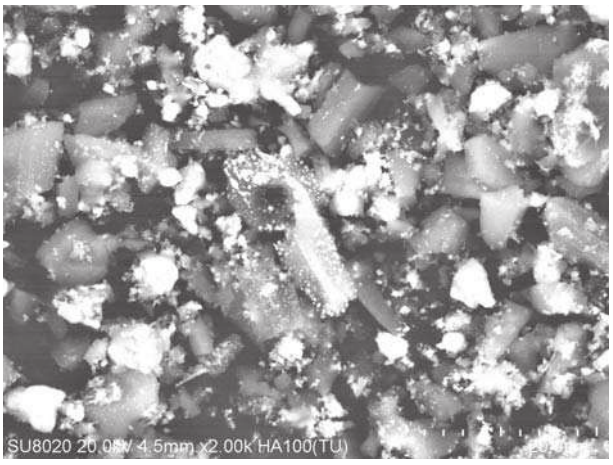

Fig. 4. Morphology of the sample No. 3. Mo-Ni-Ti-C system (40 wt.% of Ni)

3.3. EPR results

Figure 5 show asymmetric and broad EPR resonance lines, measured for sample No. 2 (Fig. 5a, T~ 54-140 K) and No. 3 (Fig. 5b, T~ 80-300 K). The first set of the lines (sample No. 2, Fig. 5a) is cantered at about 170 mT and average EPR linewidth is equal to about 350 mT, while the second one (sample 3, Fig. 5b) significantly changes its resonance positions from 210 mT to 250 mT with increasing temperature. An average EPR linewidth is equal to 315 mT. The sophisticated shape of the recorded lines indicates that the EPR resonance signal is a superposition of several signals originating from different sources (at least two). It suggests that there are a few different

magnetic centers in Mo-Ni-Ti-C sample, forming a few different magnetic phases.

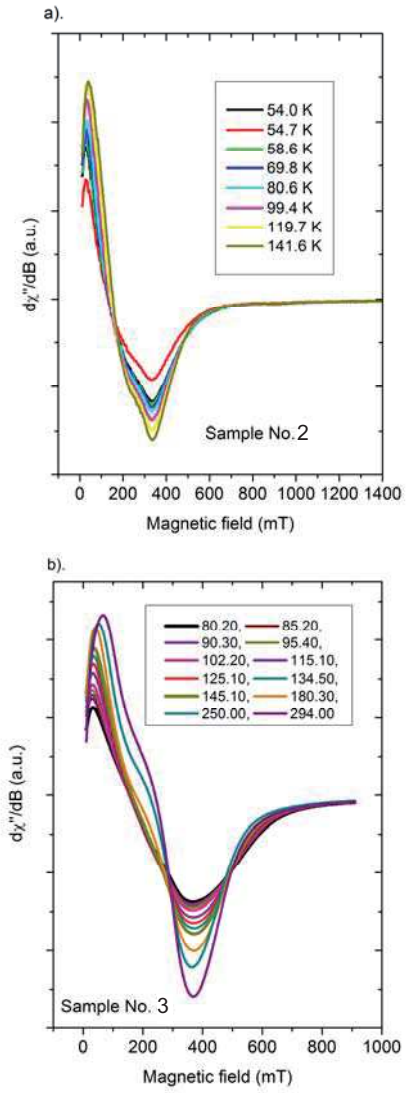

Fig. 5. Temperature dependence of EPR spectra registered for Mo-Ni-Ti-C system: a). sample No. 2, b). sample No. 3

Moreover, the intensity of the spectra increases with increasing temperature, which is an unusual feature. We have analysed the spectra calculating their integral intensity by double integration of the absorption curves (EPR susceptibility, χ_{EPR}). The linewidth and position, *g*, of the resonance lines were calculated too. The temperature dependence of the integral intensity, width and the *g*-factor of the resonance lines for sample No. 2 are presented in Figure 6, upper (a), middle (b) and lower panels (c), respectively.

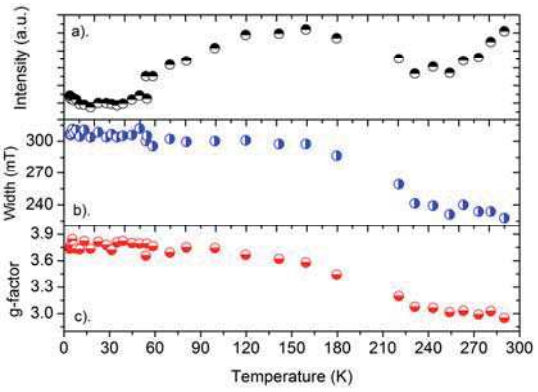

Fig. 6. Temperature dependences of the integral intensity (a), width (b) and position of the EPR resonance lines (c) for sample No. 2 (3-300 K)

As one can see the temperature dependence of integral intensity reveals the presence of some complex magnetic interactions in the Mo-Ni-Ti-C sample. It can be divided into three regions: a) from 4 to 40 K, b) from 40 to 230 K and c) above 230 K (see Fig. 6a). The linewidth remains almost constant during heating the sample from 3 K up to 160 K, with an anomaly at the temperature of 60 K, and then starts to decrease linearly as the temperature rises (see Fig. 6b). The temperature dependence of the *g*-factor behaves similarly (see Fig. 6c). The integral intensity of the Mo-Ni-Ti-C sample behaves according to the Curie-Weiss law in the low temperature region (up to ~ 40 K). The obtained Curie temperature is equal to $\Theta = -7.0 \pm 1.5$ K. A negative sign of the Curie temperature indicates the dominance of antiferromagnetic (AFM) interactions in the low temperature region.

The increase in the integral intensity of the EPR line at high temperatures region (above 230 K) suggests the dominance of EPR signals originating from transition metal ions, for example Ti^{3+}, revealing also AFM interaction. The increase and next decrease of the integral intensity appear in the middle range of temperature (40-230 K). It may indicate an occurrence of superparamagnetism phenomenon in the sample, with a blocking temperature of about 160 K. The above EPR spectra proved that the Mo-Ni-Ti-C sample contains different magnetic phases. We detected a wide range of magnetic interactions across paramagnetism, (anti)ferromagnetism and superpara-magnetism.

In Figure 7 the temperature dependences of the integral intensity, width and the *g*-factor of the resonance lines for sample No. 3 are presented in upper (a), middle (b) and lower (c) panels, respectively. They were registered in the temperature range 80-300 K. As one can see the integral

intensity (EPR susceptibility, Fig. 7a) increases with increasing temperature. This is completely inconsistent with Curie-Weiss relation expected for simple paramagnetic species. A similar increase of the relation was reported in [35] and explained by forming of ferromagnetic agglomerates. An increasing of EPR integral intensity in case of Mo-Ni-Ti-C system could be explained by a similar mechanism. As the materials doped with transition metal ions (Ti^{3+}, Ni^{3+}) are expected to possess a long-range antiferromagnetic (AFM) interactions between magnetic species [36], an increase in temperature causes destroying of overall AFM order and ferromagnetic (FM) imperfection of the structure appears. Additional discussion of this question will be presented later in the paper, after its supplementation with SQUID measurement results.

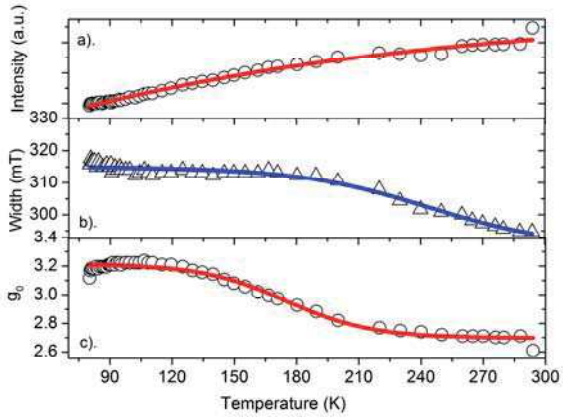

Fig. 7. Temperature dependences of the integral intensity (a), width (b) and position of the EPR resonance line (c) for sample No. 3 (80-300 K). Solid lines reflects Boltzmann curves fitted to the measured points

The linewidth of the EPR lines remains constant and equal to 315 mT with increasing temperature up to 150 K and next decreases (Fig. 7b). The resonance field is shifted from g=3.2 for 80 K to g=2.7 for 300 K (Fig. 7c), which means the shifting in magnetic field position of resonance line from 210 to 250 mT. The EPR magnetic susceptibility continuously increases with temperature increase for sample No. 3, as compared to sample No. 2, for which this increase is non-monotonic. Other temperature dependences are very similar for both samples 2 and 3.

3.4. Magnetization measurements

In Figure 8 temperature dependence of magnetic susceptibility measurements are presented for sample No. 2. Figure 9 shows hysteresis loops for the same sample registered at 52 K and 150 K. Two temperature ranges one can recognize in Figure 8: 4-25 K and 25-300 K. With temperature increase from 4 K one can observe decrease the magnetic susceptibility according to Curie-Weiss law (inset in Fig. 8). Calculated Curie temperature is equal to: Θ = -1.6 ± 0.2 K and Θ = -4.6 ± 0.5 K for FC and ZFC regimes, respectively. The negative sign of Curie temperature indicates on domination of AFM-like interactions in the temperature range 4-25 K. In a temperature range 25-300 K the magnetization increases up to reaching a broad maximum at ~240 K and next decreases up to room temperature. Such behaviour of the temperature dependence of magnetic susceptibility suggests the presence of superparamagnetism phenomenon in the Mo-Ni-Ti-C sample with blocking temperature at ~ 240 K. One can notice large difference between ZFC and FC magnetization branches for sample 2, which decreases with temperature increase. It points out on the presence of strong magnetic anisotropy. In Figure 8 we have plotted also temperature dependence of the integral EPR intensity (curve No. 2) versus temperature (see Fig. 6a). The dependence increases with increasing temperature from 25 K, next reaches maximum at about 150 K and decreases up to 240 K, where it reaches minimum. Above ~250 K it increases again with temperature increasing. The dependence is something different from temperature dependence of magnetic susceptibility measured from magnetization measurements (Fig. 8, curves 1, 2), although general shape is similar. Discrepancies observed in Fig. 8 are due to differences in technical conditions of measurements between EPR and SQUID spectroscopy. The shapes of hysteresis loops are completely different when measured for 52 K and 150 K, indicating on different kinds of magnetic interactions dominating in these temperature ranges (Fig. 9). Coercive and remnant fields are 80 Oe, 35 Oe and $1.8*10^{-3}$ emu, $1.5*10^{-3}$ emu, measured at temperatures 52 K and 150 K, respectively.

In Fig. 10 magnetizations results are presented for sample No. 3. In Fig. 11 hysteresis loops are presented for the same sample registered at 90 K, 160 K and 290 K. Two temperature ranges one can recognize in Fig. 10: 4 - 55 K and 55 – 300 K, similarly as in Fig. 8, but the ranges are something different. Therefore the sample No. 3 should has different composition compared to sample 2. Also differences between values of magnetization measured in FC and ZFC regimes are larger (about ten times) compared to sample No. 2. It means much higher magnetic anisotropy of sample 3. With temperature increase from 4 K one can observe decrease of magnetization, according to Curie-Weiss law (inset in Fig. 10). Calculated Curie temperature is equal to: Θ = -21.8 ± 1.0 K and Θ = -6.5 ± 0.4 K for FC and ZFC regimes, respectively. Negative value of Curie

temperature indicates on domination of AFM-like interactions in temperature range 4-55 K. The strange of AFM interactions (Curie temperature) is much higher compared to sample No. 2. In temperature range 55-300 K the magnetization increases up to reaching broad maximum at ~210 K and next decreases up to room temperature. Such temperature dependence of magnetic susceptibility suggests presence of superparamagnetism phenomenon in the Mo-Ni-Ti-C sample with blocking temperature at ~ 210 K.

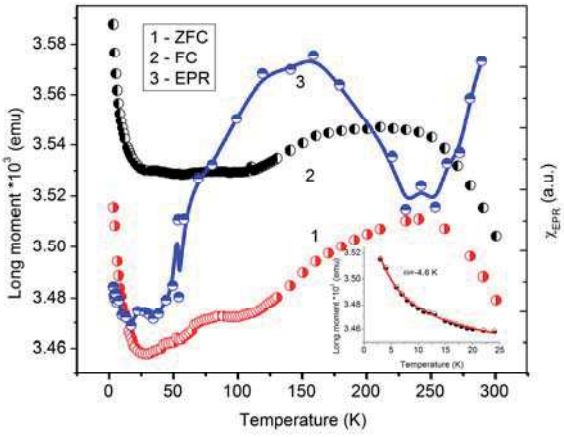

Fig. 8. Magnetic susceptibility of sample 2 measured in FC (2) and ZFC (1) regimes in magnetic field H=1000 Oe. Curve 3 reflects integral intensity, χ_{EPR}, of EPR spectra (Fig. 6a). Inset shows magnetization ZFC curve in temperature range 4-25 K. Solid line represents fit to Curie-Weiss law

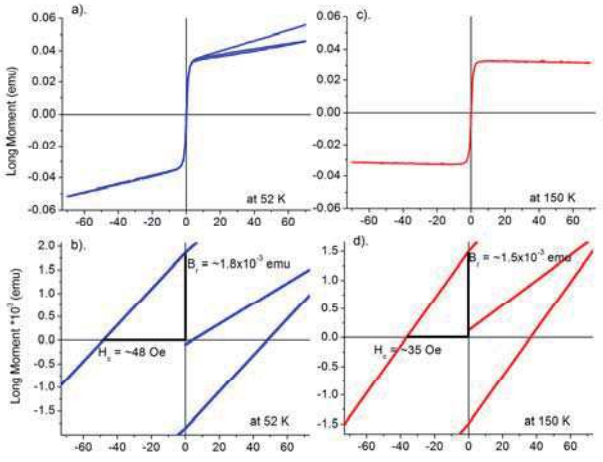

Fig. 9. Hysteresis loops measured for sample No. 2 at a temperatures a). 52 K and c). 150 K. Fig. 9b) and 9d). shows enlargements of the loops near zero field measured at 52 K and 150 K, respectively

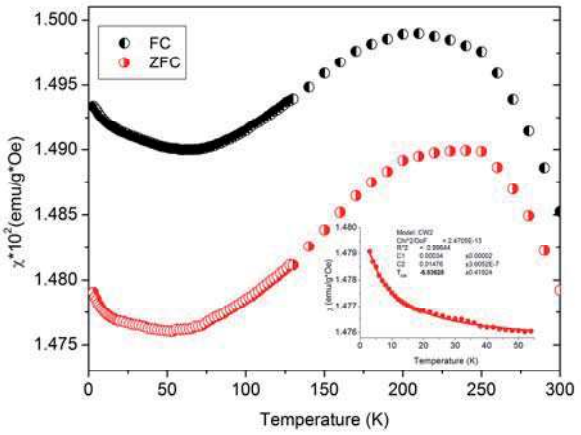

Fig. 10. Magnetic susceptibility of sample 3 measured in FC and ZFC regimes in magnetic field H=1000 Oe. Inset shows magnetization enlarged in temperature range 4-55 K. Solid line represents fit to Curie-Weiss law

The increase of magnetic susceptibility with increasing temperature (Fig. 10) could be explained by appearing of AFM structure in the investigated samples. According to earlier reports concerning similar kind of steel [35], such materials possess specific magnetic composition. In these materials minority of FM components occur as an imperfection in overall AFM structure. Thus, AFM ordering is destroyed with increasing temperature and overall magnetization is enhanced. This phenomenon may be due to the presence of magnetic nanoparticles in Mo-Ni-Ti-C samples.

The results of hysteresis loops measurements recorded at a temperature of 160 K (below blocking temperature) and 290 K (above blocking temperature) for sample 3 (Fig. 11) show that magnetic hysteresis appear in the investigated sample both below and above blocking temperature.

The hysteresis loops are very thin. They have low coercive field and remnant parameters. Coercive and remnant parameters measured at T=90 K we calculated as: H_c=~37 Oe and B_r=10*10^{-3} emu (Fig. 11). For higher temperatures the values decrease (see Fig. 11) with temperature decrease. The presence of hysteresis loop is strong evidence of (anti)ferromagnetic interaction occurring in a sample. However, it should be noticed that appearing of magnetic hysteresis and (anti)ferromagnetic interaction does not disprove existence of superparamagnetism phenomenon. The Mo-Ni-Ti-C sample is built of few magnetic phases that show: a) paramagnetic properties, dominating from helium temperatures up to a temperature of 55 K, b) superparamagnetic properties,

dominating in the temperature range 55-300 K and c) ferromagnetic properties, observed at temperatures above 55 K.

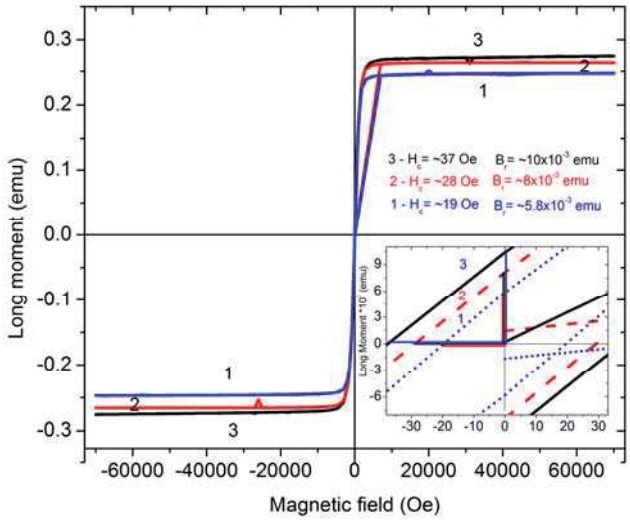

Fig. 11. Hysteresis loops measured for sample No. 4 at temperatures of 90 K (3), 160 K (2) and 290 K (1). Inset shows enlargement of hysteresis loops for magnetic fields near zero value

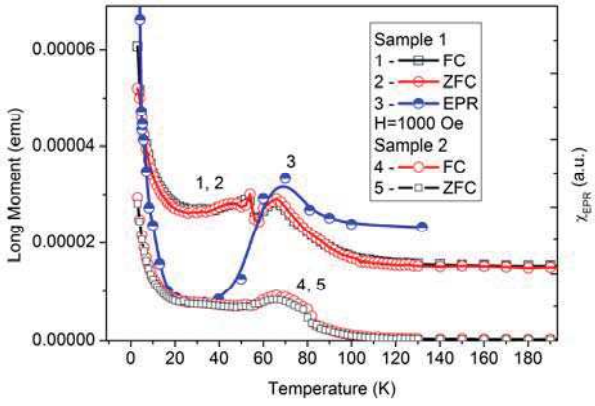

Fig. 12. Temperature dependences of magnetic properties of sample No. 1 (curves 1, 2 and 3) and sample No. 2 (curves 4 and 5). Curve No. 3 shows EPR integral intensity, χ_{EPR}, calculated for sample No. 1

To confirm the dependence of magnetic properties of Mo-Ni-Ti-C systems on phase composition we present in Figure 12 results of magnetic measurements for two samples presented in Table 1 (curves 1, 2,3 for sample No. 1 and 4, 5 for sample No. 2, respectively). As one can see changes in magnetic susceptibility of both samples are much less than these observed for samples No. 3. Moreover, there is not observed a difference between magnetization in FC and ZFC regimes. High magnetic anisotropy is absent in case of samples 1 and 2. EPR investigations (curve 3 for sample No. 1) confirm magnetic properties obtained based on magnetization measurements.

4. Conclusions

The results obtained in the present study lead to the following conclusions

- The magnetic susceptibility and EPR measurements confirm the presence of magnetic ions (Ti^{3+} and Ti^{2+}) in Mo-Ni-Ti-C samples, forming different magnetic phases, as e.g. (Mo,Ti)C, C, Ni. They create different magnetic interactions like:
  a) paramagnetism,
  b) antiferromagnetism and ferromagnetism,
  c) superparamagnetism.
- The Mo-Ni-Ti-C samples are magnetically dense. They contain nanoparticles, that may form agglomerates.
- It seems that different phases are responsible for paramagnetism and antiferromagnetism in the samples.
- Nanoparticles may be responsible for superpara-magnetism.
- Selection of different phases allow to influence magnetic properties of the investigated system and create fixed, dominating kind of magnetic interactions. Appropriate choice of magnetic phases can play a fundamental role in further, practical applications of Mo-Ni-Ti-C systems.

References

[1] R.W. Siegel, Nanostructure Science and Technology. A Worldwide Study; in: R.W. Siegel, E. Hu, M.C. Roco (Eds.), R&D Status and Trends in Nanoparticles, Nanostructured Materials, and Nanodevices, Report, WTEC, Loyola College in Maryland, 1999.

[2] H. Gleiter, Nanostructured materials: State of the art and perspectives, Nanostructured Materials 6 (1995) 3-14.

[3] A.S. Edelstein, R.C. Cammarata (Eds.), Nano-materials: Synthesis, properties and applications, IOP, Bristol, 1996.

[4] R.W. Siegel, Nanophase materials, in: G.L. Trigg (Ed.), Encyclopedia of applied physics, Vol. 11, VCH, Weinheim, 1994, 1-27.

[5] N.A. Frey, S. Peng, K. Cheng, S. Sun, Magnetic nanoparticles: Synthesis, functionalization and applications in bioimaging and magnetic energy storage, Chemical Society Reviews 38 (2009) 2532-2542.
[6] M.H. Pablico-Lansigan, S.F. Situ, A.C.S. Samia, Magnetic particle imaging: advancements and perspectives for real-time in vivo monitoring and image-guided therapy, Nanoscale 5 (2013) 4040-4055.
[7] R.D. Shull, R.D. McMichael, L.J. Schwartendruber, L.H. Bennett, Magnetocaloric effect of ferromagnetic particles, Proceedings of the 7th International Cryocoolers Conference, 1992.
[8] I. Koh, L. Josephson, Magnetic nanoparticle sensors, Sensors 9 (2009) 8130-8145.
[9] T.A.P. Rocha-Santos, Sensors and biosensors based on magnetic nanoparicles, Trends in Analytical Chemistry 62 (2014) 28-36.
[10] S. Bednarek, Ferromagnetic fluids – materials with unusual properties and their applications, Foton 104 (2009) 22-29 (in Polish).
[11] A. Hervault, N.T.K. Thanh, Magnetic nanoparticle-based therapeutic agents for thermo-chemotherapy treatment of cancer, Nanoscale 6 (2014) 11553-11573.
[12] N. Huilgol (Ed.), Hyperthermia, Proceedings of the INTECH 2013, Morn Hill, 2013.
[13] M.Y. Razzaq, M. Behl, A. Lendlein, Memory-effects of magnetic nanocomposites, Nanoscale 4 (2012) 6181-6195.
[14] D. Pinkowicz, H. Southerland, X.-Y. Wang, K.R. Dunbar, Record Antiferromagnetic Coupling for a Cyanide-Bridged Compound, Journal of the American Chemical Society 136 (2014) 9922-9924.
[15] R.V. Mambrini, T.L. Fonseca, A. Dias, L.C.A. Oliveira, M.H. Araujo, F.C.C. Moura, Magnetic composites based on metallic nickel and molybdenum carbide: A potential material for pollutants removal, Journal of Hazardous Materials 241-242 (2012) 73-78.
[16] Z.H. Wang, D. Li, D.Y. Geng, S. Ma, W. Liu, Z.D. Zhang, The characterizations of superconducting MoC/Mo_2C nanocomposites embedded in a magnetic graphite matrix, Physica Status Solidi A 205/12 (2008) 2919-2923.
[17] C.I. Sathish, Y. Guo, X. Wang, Y. Tsujimoto, J. Li, S. Zhang, Y. Matsushita, Y. Shi, H. Tian, H. Yang, J. Li, K. Yamaura, Superconducting and structural propertiesof d-$MoC_{0.681}$ cubic molybdenum carbide chase, Journal of Solid State Chemistry 196 (2012) 579-585.
[18] Y. Yanaba, T. Takahashi, K. Hayashi, A consideration on TiC-core/(Ti,Mo)C-rim structure of TiC-Mo_2C-Ni cermet in relation to hypothesis "Exhaustion of diffusion-contributable atomic vacancies in core/rim structure", Journal of the Japan Society of Powder and Powder Metallurgy 51/5 (2004) 374-384.
[19] R. Ohser-Wiedemann, C. Weck, U. Martin, A. Müller, H. J. Seifert, Spark Plasma Sintering of TiC particle-reinforced molybdenum composites, International Journal of Refractory Metals and Hard Materials 32 (2012) 1-6.
[20] M.M. Kulak, B.B. Khina, Self-propagation high-temperature synthesis in the Ti-C-Ni-Mo system on application of powerful ultrasound, Journal of Engineering Physics and Thermophysics 87/2 (2014) 333-343.
[21] J. Qin, I. Asempah, S. Laurent, A. Fornara, R.N. Muller, M. Muhammed, Injectable superparamagnetic ferrogels for controlled release of hydrophobic drugs, Advanced Materials 21 (2009) 1354-1357.
[22] V.N. Eremenko, T.Y. Velikonova, Phase equilibria in the Mo-TiC-Ti of the ternary system Mo-Ti-C. Character of solidification of alloys and projection of the solidus surface, Powder Metallurgy and Metal Ceramics 8/11 (1969) 931-936.
[23] K. Takagi, K. Osada, W. Koike, T. Fujima, Effect of Mo_2C content on the properties of TiC/TiB_2 base cermets, Journal of Physics: Conferences Series 176 (2009) 012044.
[24] J. Zackrisson, A. Larsson, H.-O. Andren, Micro-structure of the Ni binder phase in a TiC-Mo_2C-Ni cermet, Micron 32 (2001) 707-712.
[25] Y.K. Kim, J.-H. Shim, Y.W. Cho, H.-S. Yang, J.-K. Park, Mechanochemical synthesis of nanocomposite powder for ultrafine (Ti, Mo)C-Ni cermet without core-rim structure, International Journal of Refractory Metals & Hard Materials 22 (2004) 193-196.
[26] J.I. Keene, Characterization of a Ti(Mo)C-Ni cermet for use in impact resistant sandwich panels, A Thesis Presented to the faculty of the School of Engineering and Applied Science University of Virginia, December 2013, http://www.virginia.edu/ms/research/wadley/Thesis/JKeeneMS.pdf; 15.06.2015,
[27] Y.F. Yang, S.B. Jin, Q.C. Jiang, Effect of reactant C/Ti ratio on the stoichiometry, morphology of TiC_x and mechanical properties of TiC_x–Ni composite, Crystal Engineering Communications 15 (2013) 852-855.
[28] T. Viatte, T. Cutard, G. Feusier, W. Benoit, High temperature mechanical properties of Ti(C, N)-Mo_2C-Ni cermets studied by internal friction measurements, Journal de Physique IV, Colloque C8, suppltment au Journal de Physique III 6 (1996) 743-746.

[29] M.A. Qian, L.C. Lim, On the disappearance of Mo_2C during low-temperature sintering of Ti(C,N)-Mo_2C-Ni cermets, Journal of Materials Science 34 (1999) 3677-3684.
[30] J.C. LaSalvia, D.K. Kim, R.A. Lipsett, M.A. Meyers, Combustion Synthesis in the Ti-C-Ni-Mo System: Part I, Micromechanisms, Metallurgical and Materials Transactions A 26 (1995) 3001-3009.
[31] M. Viljus, J. Pirso, K. Juhani, S. Letunovits, Structure Formation in Ti-C-Ni-Mo Composites during Reactive Sintering, Materials Science 18/1 (2012) 62-65.
[32] C. Wenlin, L. Ning, C. Sheng, Effect of titanium carbide addition on microstructure and mechanical properties of ultra-fine Ti(C, N)–Ni cermet, Journal of the Chinese Ceramic Society 35/9 (2007) 1210-1216.
[33] A. Biedunkiewicz, P. Figiel, M. Krawczyk, U. Gabriel-Półrolniczak, S. M. Kaczmarek, T. Bodziony, T. Skibiński, Material in form powder with magnetic properties and method of manufacturing of the material in form powder, Polish Patent P 413627, 2015 (in Polish).
[34] P. Scherrer, Bestimmung der Grösse und der inneren Struktur von Kolloidteilchen mittels Röntgenstrahlen, Nachrichten von der Gesellschaft der Wissenschaften zu Göttingen 26 (1918) 98-100 (in German).
[35] N. Guskos, J. Typek, M. Maryniak, U. Narkiewicz, W. Arabczyk, I. Kucharewicz, Temperature dependence of FMR spectrum of Fe_3C magnetic agglomerates, Journal of Physics: Conferences Series 10 (2005) 151-154.
[36] J. Crangle, A. Fogarty, M.J. Taylor, Weak ferromagnetism in 'non-magnetic' austenitic stainless steel, Journal of Magnetism and Magnetic Materials 111 (1992) 255-259.